Local and Nonlocal Optically Induced Transparency Effects in Graphene–Silicon Hybrid Nanophotonic Integrated Circuits

Longhai Yu,[†,⊥] Jiajiu Zheng,[†,⊥] Yang Xu,[‡] Daoxin Dai,[*,†] and Sailing He[*,†,§]

[†]Centre for Optical and Electromagnetic Research, JORCEP, State Key Laboratory for Modern Optical Instrumentation, Zhejiang Provincial Key Laboratory for Sensing Technologies, Zhejiang University, Hangzhou 310058, China, [‡]Department of Information Science and Electronic Engineering, Zhejiang University, Hangzhou 310027, China, and [§]Department of Electromagnetic Engineering, School of Electrical Engineering, Royal Institute of Technology, S-100 44 Stockholm, Sweden. [⊥]These authors contributed equally to this work.

ABSTRACT Graphene is well-known as a two-dimensional sheet of carbon atoms arrayed in a honeycomb structure. It has some unique and fascinating properties, which are useful for realizing many optoelectronic devices and applications, including transistors, photodetectors, solar cells, and modulators. To enhance light–graphene interactions and take advantage of its properties, a promising approach is to combine a graphene sheet with optical waveguides, such as silicon nanophotonic wires considered in this paper. Here we report *local* and *nonlocal* optically induced transparency (OIT) effects in graphene–silicon hybrid nanophotonic integrated circuits. A low-power, continuous-wave laser is used as the pump light, and the power required for producing the OIT effect is as low as ~0.1 mW. The corresponding power density is several orders lower than that needed for the previously reported saturated absorption effect in graphene, which implies a mechanism involving light absorption by the silicon and photocarrier transport through the silicon–graphene junction. The present OIT effect enables low power, all-optical, broadband control and sensing, modulation and switching *locally* and *nonlocally*.

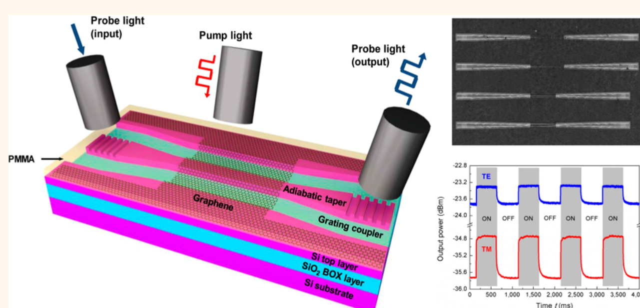

KEYWORDS: graphene · optically induced transparency · local and nonlocal · silicon · low power

Graphene has attracted extensive interest since its discovery in 2004 due to many unique optoelectronic properties,[1–4] such as carrier mobility as high as 200 000 $cm^2\ V^{-1}\ s^{-1}$ at room temperature,[5,6] zero-bandgap and electrochemically tunable Fermi level,[4,7] broadband absorption of $\pi\alpha = \sim 2.3\%$ per layer for vertically incident light,[3,4] giant Kerr constants and other large optical nonlinearities.[8,9] Leveraging these properties of graphene can produce novel architectures and performance in many devices and applications, like transistors,[10,11] photodetectors,[12,13] solar cells,[14,15] modulators,[16,17] and saturable absorbers.[18,19]

The two-dimensional nature of graphene makes it challenging to design optical systems that take advantage of its properties. Putting a graphene sheet on top of an optical waveguide forms a kind of hybrid optical waveguide. This device geometry extends the light-matter interaction to the length of the hybrid optical waveguide and on-chip graphene devices can be realized. Since silicon photonics has been developed extensively for many applications,[20,21] it is appealing to combine graphene and silicon-on-insulator (SOI) nanowires to form graphene–silicon hybrid nanophotonic wires so that active silicon photonic devices become available. This hybrid integrated platform has been previously used to realize on-chip active silicon photonic devices such as graphene electro-absorption modulators,[16,17] waveguide-type graphene photodetectors,[22–24] and some other photonic devices.[25,26]

In this paper, a *local* and *nonlocal* optically induced transparency (OIT) effect in

* Address correspondence to sailing@kth.se, dxdai@zju.edu.cn.

Received for review August 6, 2014 and accepted November 5, 2014.

Published online November 05, 2014
10.1021/nn504377m

© 2014 American Chemical Society

graphene–silicon hybrid photonic integrated circuits is demonstrated for the first time, which enables all-optical modulation over a broad wavelength range. Illuminating the graphene sheet as far as 4 mm away from the hybrid nanophotonic wire produced substantial modulation of the transparency. The present OIT effect is different from the saturated absorption effect in graphene reported previously.[18,19] For the saturated absorption effect, the graphene absorption was *locally* reduced at the position where the graphene sheet is illuminated by light, with an optical power density of up to 0.5–0.7 × 10^6 W/cm^2 from a high-power femtosecond laser.[18,19,25] In contrast, in the present work a low-power continuous-wave laser is used and the power density to produce the OIT effect is extremely low, only ~2 W/cm^2, which can be achieved with carriers being generated in the silicon layer and injected into the graphene layer. In this paper we demonstrate this lower power, all-optical, *local* and *nonlocal* OIT effect through a series of experimental measurements.

RESULTS AND DISCUSSION

The waveguide consists of an input and output grating couplers with a single mode 520 nm × 240 nm silicon core region. The silicon layer is slightly p-type doped (with a concentration of ~3 × 10^{14} cm^{-3}). A monolayer graphene sheet grown by chemical vapor deposition (CVD) is wet-transferred onto the SOI chip,[27] and then patterned by an oxygen plasma etching process to expose the grating couplers as schematically seen in Figure 1a. Figure 1b is an SEM image showing the fabricated graphene–silicon hybrid nanophotonic wires with different lengths (L = 100, 120 μm in the figure). The left inset in Figure 1b shows a zoom-in top view for a graphene–silicon hybrid nanophotonic wire. Although there are a few noticeable small air voids in the regions around the sidewalls due to the stepped surface, the wet-transferred graphene sheet contacts the SOI-nanowire chip very well. The right inset shows a zoom-in view for the boundary of the patterned graphene. The measured propagation losses for the probe light (λ = 1560 nm) propagating along the graphene–silicon hybrid nanophotonic wires were measured as ~0.106 and ~0.175 dB/μm for TE- and TM-polarization modes, respectively, which are shown by their optical field distributions in Figure 1c. The measured propagation losses, which are mainly from the graphene absorption, are consistent with the theoretical values (~0.11 dB/μm for TE and ~0.17 dB/μm for TM) calculated with a finite element simulation (FEM) mode-solver (see Supporting Information).

The dynamic response of the probe light (λ = 1560 nm) is measured when a modulated 635 nm continuous-wave laser is used as the pump light to illuminate the chip vertically through an optical fiber (see Figure 1a). The position of the pump light is on top

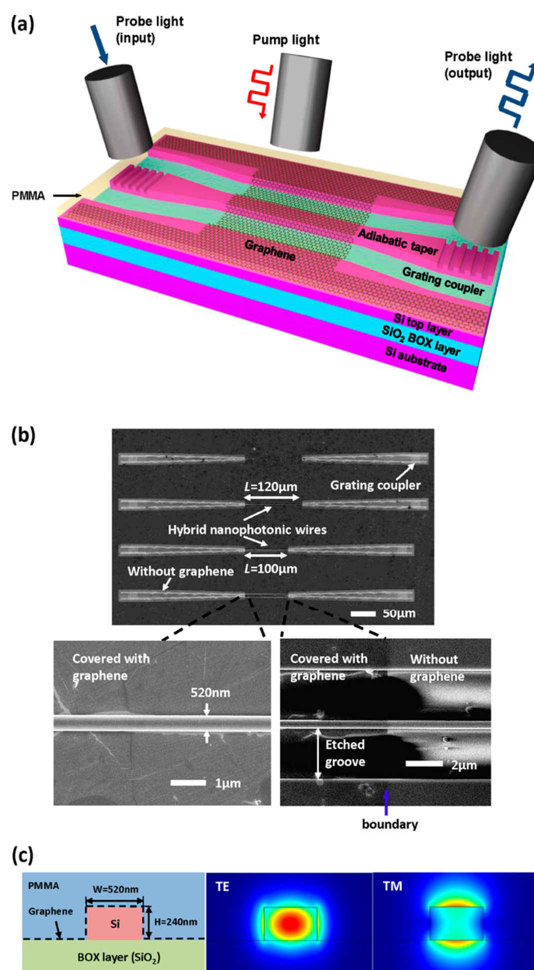

Figure 1. (a) Three-dimensional schematic illustration of a graphene–silicon hybrid nanophotonic wire. The probe light is coupled into and out of the SOI nanowire by using grating couplers with adiabatic tapers. The pump light is emitted through a fiber on top of the SOI-nanowire. (b) Top-view SEM image of graphene–silicon hybrid nanophotonic wires fabricated by two grooves. Graphene on top of the grating couplers and the adiabatic tapers (see the light-gray regions) was removed with the oxygen plasma etching process (scale bar: 50 μm). Left inset, a zoom-in view for the hybrid nanophotonic wire (scale bar: 1 μm). Right inset, a zoom-in view for the boundary of the patterned graphene at the junction of the hybrid nanophotonic wire and the adiabatic taper (scale bar: 2 μm). (c) Left: the cross section of a hybrid nanophotonic wire. Middle and right: the optical mode profiles of TE- and TM-polarization modes, respectively.

of the hybrid nanophotonic wires, which is called the local illumination (as shown in Figure 2a). The diameter of the pump light spot on the chip surface is about 90 μm while the pump power is 15 mW. When the modulation frequency of the pump light is 1 Hz with a duty cycle of 0.5, the response for TE- and the TM-polarization modes are shown in Figure 2b. It can be seen that the output power of the probe light increases for both polarizations when the pump light is "ON", indicating that there is less loss in the graphene–silicon nanophotonic wires, which is called the OIT effect here. The modulation depth for the OIT effect is defined as the loss reduction, and the modulation

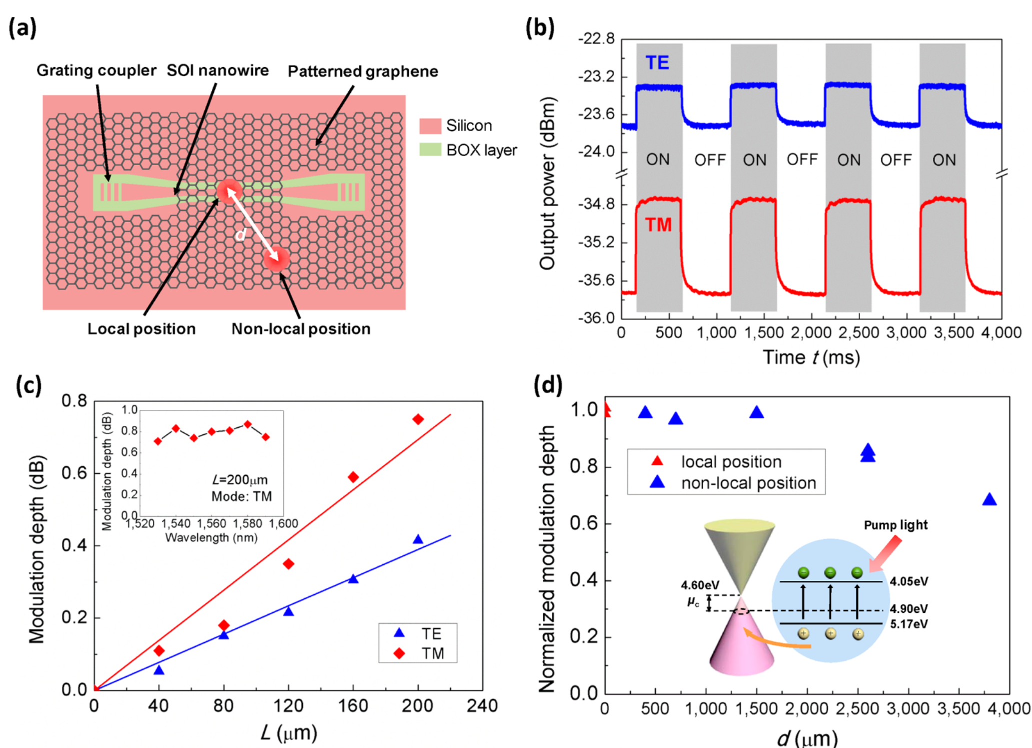

Figure 2. (a) Schematic diagram of local and nonlocal positions for the pump light illumination. (b) Dynamic responses of the output power for TE- and TM-polarization modes of hybrid nanophotonic wires with a modulated optical pump locally. (c) Modulation depths of the hybrid nanophotonic wires with varying lengths (measured by using another sample with the same design and the fabrication processes). Inset, the dependence of the modulation depth on the probe wavelength for TM-polarization mode in a 200 μm-long hybrid nanophotonic wire. (d) Normalized modulation depths at nonlocal positions as distances d varies. Inset, schematic diagram of energy levels of graphene and silicon, as well as carrier transport at their interface under light illumination.

depths are respectively about 0.4 and 1.0 dB for TE- and TM-polarizations when the length of the hybrid nanophotonic wire is $L = 200\ \mu$m in the present example (see Figure 2b). In Figure 2c, the modulation depth is shown as the length L varies from 0 to 200 μm. It can be seen that the modulation depth for both polarizations increases linearly with length L. Particularly, for the case of $L = 0$ (*i.e.*, without graphene on top of SOI nanowires), there is no change for the output power of the probe light when the pump light switches between "ON" and "OFF" states, indicating that graphene is necessary for the present OIT effect. The dependence of the modulation depth on the probe light wavelength is also characterized as shown in the inset of Figure 2c, from which it can be seen that the response is quite flat over the wavelength range from 1,520 nm to 1,600 nm.

We also measured the loss of the hybrid nanophotonic wires with a nonlocal illumination of pump light. The position of the pump light is moved to the graphene far away from the hybrid nanophotonic wires, as shown in Figure 2a. Figure 2d shows the measured modulation depth *versus* the distance d of the nonlocal illumination position away from the local-illumination position, normalized to the local-illumination case. From Figure 2d, it can be seen that the OIT effect is still significant even when it is with nonlocal illumination of pump light. The modulation depth decreases slightly as the distance d increases. Even when the distance d increases to ~4 mm, the nonlocal modulation depth is still 68% of the local modulation depth. Such a nonlocal OIT effect opens a way to the realization of remote all-optical manipulation.

For the local case with the 635 nm pump light, the pump light is absorbed by the graphene layer, the silicon layer as well as the silicon substrate, generating photocarriers in the three regions. The carriers generated in the silicon substrate do not influence the loss of the probe light propagating along the hybrid nanophotonic wire because silicon substrate is optically and electrically isolated in the SOI device geometry. In contrast, the carriers generated in the silicon layer would introduce some free carrier absorption (FCA) loss depending on the free carrier concentration.[28,29] For the present case, there is no FCA loss observed for the probe light propagating along the SOI nanowire without graphene when the pump light is "ON" with a power of 15 mW, indicating that the FCA loss in the silicon layer is negligible (which is consistent with the theoretical estimation) because the carrier concentration is low here. Since we have observed loss reduction (instead of loss increase) in the experiment as shown in Figure 2b, the OIT effect should not directly come from the variation of carrier concentration in the

silicon layer. This is also verified by the measurement result for the nonlocal case (shown in Figure 2d), where the carriers in the silicon layer are far away and isolated from the silicon core region of the hybrid nanophotonic wire (see Figure 2a).

Previously, people have demonstrated the so-called saturated absorption effect (with reduced material absorption at a high optical power level) in a graphene sheet by using an ultrahigh power pulse laser,[18,19] and the optical power density is usually up to $(0.5-0.7) \times 10^6$ W/cm^2. In contrast, the power density to produce the OIT effect is as low as ~230 W/cm^2 for our present measurement with 15 mW pump light whose spot diameter is about 90 μm. Actually, the power density required can be much smaller (~2 W/cm^2), which will be shown in our experiments below. It can be seen that the power density to produce the present OIT effect is several orders lower than that for the saturated absorption effect, which indicates that they have different mechanisms.

Note that a Schottky diode is formed when a graphene sheet is put on top of a silicon layer.[14,15,30] The energy diagram is given in the inset of Figure 2d. Correspondingly, the Fermi level of the slight p-type doped silicon (with a concentration of $\sim 3 \times 10^{14}$ cm^{-3} characterized by the SIMS measurement shown in Supporting Information) used here is ~4.90 eV.[31] The Dirac point of graphene is ~4.60 eV,[32] and the CVD-grown graphene in our case is p-type doped with a chemical potential $\mu_c \approx -0.27$ eV, which is estimated from the Raman spectra of graphene and the propagation losses of the hybrid nanophotonic wires (see Supporting Information for details).[24,26,30,33,34] When light illuminates the diode and some nonequilibrium carriers are generated, there is carrier transport between the graphene sheet and the silicon layer. For the present case, when the 635 nm pump light illuminates the diode, photocarriers are generated in the silicon layer as well as the graphene layer at the illumination area. Since CVD-grown graphene usually has a high carrier mobility of $\sim 10^3$ cm^2 V^{-1} s^{-1} at room temperature after fabrication processes,[27,35] photocarriers generated in graphene will transport from the illumination area to the whole graphene sheet quickly and consequently the carrier concentration in graphene becomes lower than that in the silicon layer in the illumination area. As a result, the photocarriers generated in the silicon layer will move to the graphene sheet through the Schottky diode junction. Some electrons are likely trapped at the interface due to the impurity and defect effect,[36] and finally the stable carrier concentration of the whole p-type doping graphene sheet in our case becomes high. And then the chemical potential $|\mu_c|$ of graphene increases, which is equivalent to a lower Fermi level (according to the definition for the chemical potential $|\mu_c|$) for p-type doping graphene (see Supporting Information). A lower Fermi level for p-type doping graphene implies a higher interband transition energy, and thus the absorption of graphene is suppressed (similar to the case of small negative drive voltage in Figure 2 of ref16). The modulation depth achieved in this paper is ~1 dB over 200 μm or 0.005 dB/μm, which is consistent with the values for the electrically induced transparency for shifting the Fermi level at energies lower than excitation light.[16] Achieving a significantly larger modulation should be possible through judicious doping of the graphene or silicon to place the initial Fermi level outside of this region and put it into the region with sharp variation of graphene absorption (such as the case of big negative or positive drive voltage in Figure 2 of ref 16).

To verify that the OIT effect requires the carrier transport between the silicon layer and the graphene sheet, we did more measurements with 15 mW pump light illumination at different positions *A*, *B*, *C*, and *D*, where the layered structures are different as shown in Figure 3a. The corresponding measured powers of the probe light output from a 200 μm-long hybrid nanophotonic wire are shown in Figure 3b. From this figure, it can be seen that similar modulation depths are achieved for local position *A* and nonlocal position *B* (which has been shown in Figure 2d). In contrast, the modulation depth is suppressed significantly as shown by the red curve in Figure 3b when the pump light is illuminating nonlocal position *C*, where the silicon layer in a 200 μm × 200 μm square window is removed. This indicates that the photocarriers generated in the silicon layer is essential for producing the present OIT effect. When the silicon layer is removed, the carriers in the graphene sheet are generated from the pump-light absorption in graphene only. In this case, the carrier concentration in the graphene layer is too low to generate the OIT effect. However, we can still observe a small modulation depth (see the red curve in Figure 3b) because some scattering/diffraction at the fiber end helps a small part of the pump light to illuminate the silicon layer in the area outside of the 200 μm × 200 μm square window, generating some photocarriers. This has been also verified by lifting the fiber for the pump light in our experiment. When the fiber for the pump light is lifted, we observed a larger modulation depth (not shown here) because the spot size of the pump light increases and more power is absorbed by the silicon outside of the square window.

When the pump light is moved to illuminate nonlocal position *D*, where there is a 20 nm-thick SiO_2 insulating layer between the silicon layer and the graphene sheet, no OIT effect is observed (see the purple curve in Figure 3b). Here the SiO_2 insulating layer blocks the "channel" for the carrier transport between the silicon layer and the graphene sheet. From the comparison shown in Figure 3b, it can be seen that the generation of photocarriers in the silicon layer and

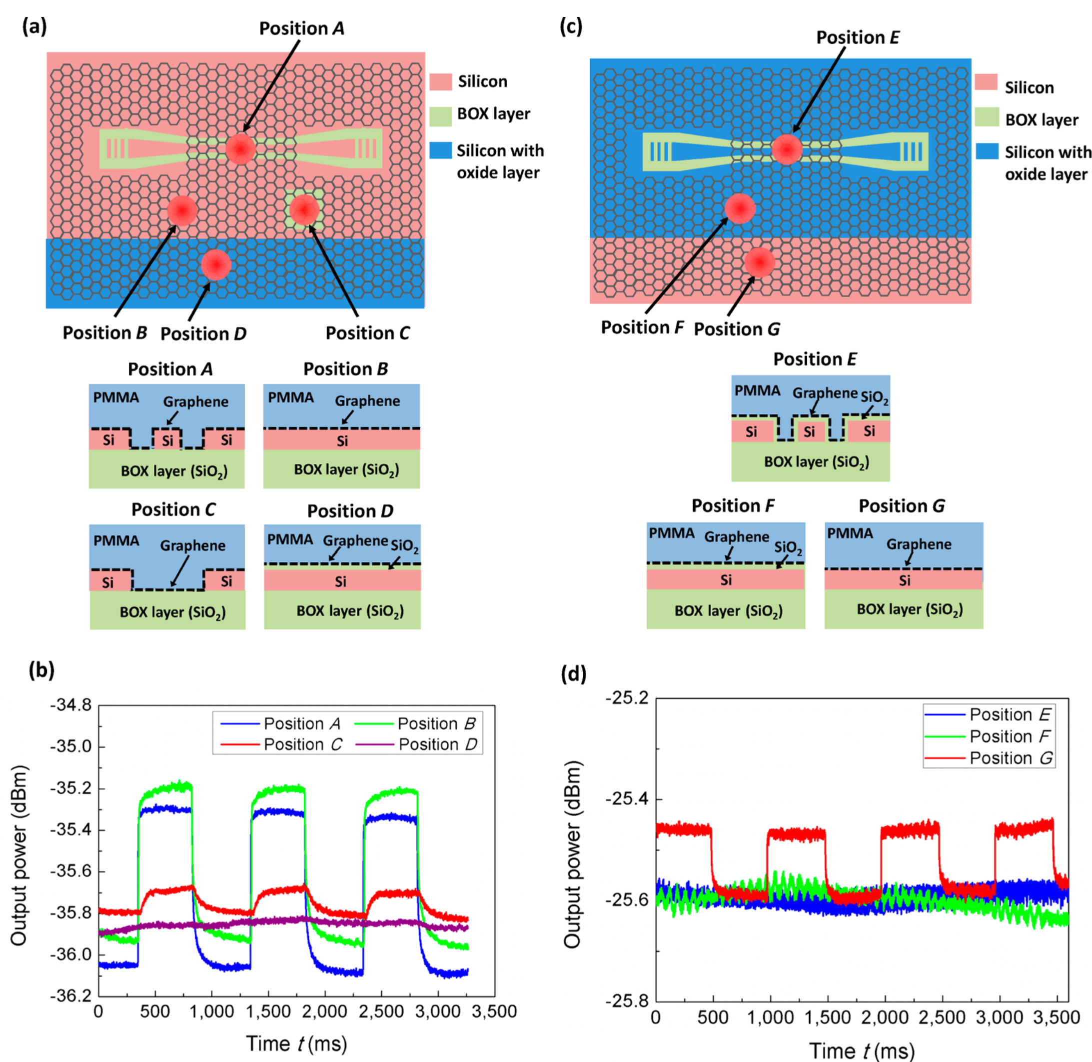

Figure 3. (a) Top, positions *A*, *B*, *C*, and *D* on one chip for the pump light illumination. Bottom, the cross sections for these illumination positions. (b) Measured dynamic responses for positions *A*, *B*, *C*, and *D*. (c) Top, positions *E*, *F*, and *G* on one chip for the pump light illumination. Bottom, the cross sections for these illumination positions. (d) Measured dynamic responses for illumination positions *E*, *F*, and *G*. Here the pump light power is 15 mW.

the carrier transport through the silicon-graphene junction is necessary for the present OIT effect.

We have also fabricated some hybrid nanophotonic wires with a 20 nm-thick SiO_2 insulating layer between the silicon layer and the graphene sheet, as shown in Figure 3c. The measurements were done by illuminating the chip with the pump light at different positions *E*, *F*, and *G*. There is a 20 nm-thick SiO_2 insulating layer at local position *E* and nonlocal position *F*, while there is no SiO_2 insulating layer at nonlocal position *G*, as shown in Figure 3c. The measurement results for the modulation depth of the probe light are shown in Figure 3d. It can be seen that there is no observable OIT effect when the pump light illuminates positions *E* and *F*. In contrast, the OIT effect was observed with nonlocal illumination at position *G*. From the comparison between positions *F* and *G*, it is further verified that the carrier transport through the silicon-graphene junction is the key process in producing the present OIT effect. One can eliminate the OIT effect completely by blocking the carrier transport with a thin SiO_2 insulator layer.

According to the analyses for Figures 2 and 3 above, the mechanism of the present OIT effect is described as follows. The pump light is absorbed and photocarriers are generated in the silicon layer as well as the graphene sheet at the illumination area. The carrier concentration in the entire graphene sheet is enhanced due to the photocarrier transport through the silicon-graphene junction at the illumination position and the photocarrier transport in the graphene sheet, so that a reduction of the graphene absorption (*i.e.*, OIT effect) is achieved at the graphene–silicon hybrid nanophotonic wire.

Measuring the modulation depth as a function of pump power (Figure 4a) provides insight into the potential barriers associated with the Schottky diode. It can be seen that the modulation depth increases to

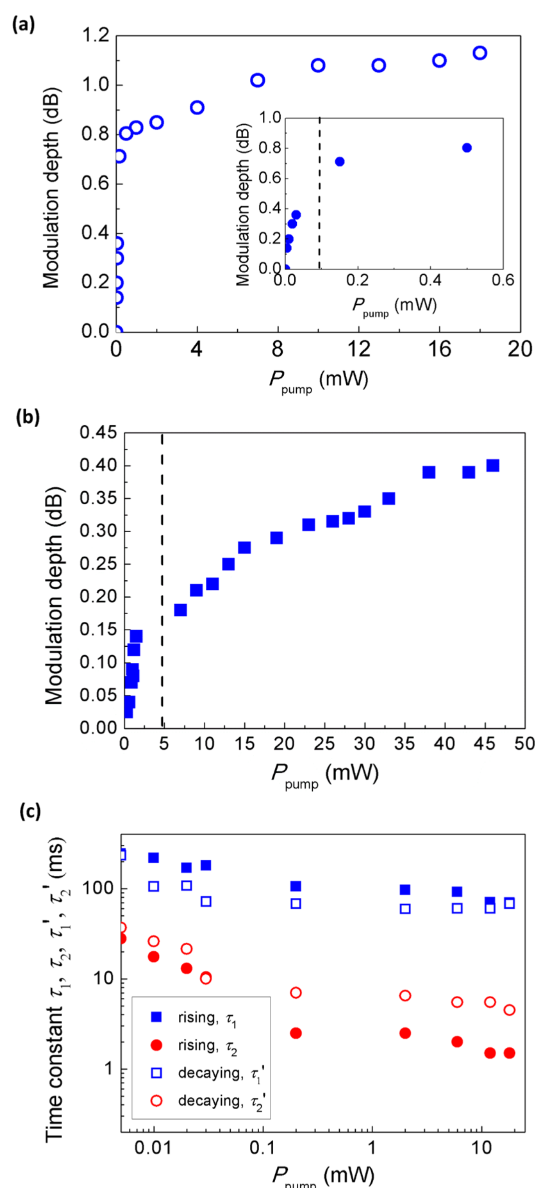

Figure 4. (a) Modulation depth as the pump power P_{pump} varies. Inset, a zoom-in view in the region of $P_{pump} < 0.6$ mW. (b) Modulation depth as the pump power P_{pump} varies when $\lambda_{pump} = 970$ nm, which is similar to that for $\lambda_{pump} = 635$ nm shown in (a). (c) The pump-power dependence of the fitted time constants τ_1, τ_2 for the rising process (closed squares/circles) and τ_1', τ_2' for the decaying process (open squares/circles).

~0.8 dB when the pump power increases from 0 to 0.1 mW. Considering the fact that the Fermi levels of graphene and silicon are slightly different, there is a small potential barrier at the interface when they come into contact to form a Schottky diode,[14,15] and the transport coefficient η_T for the carrier transport from the silicon layer to the graphene sheet is dependent on this potential barrier (see Supporting Information). When the pump power is low, the number of photocarriers generated in the silicon layer is limited and some of the photocarriers go through the barrier and inject into the graphene sheet. Consequently, the doping in the graphene sheet becomes higher, and the Fermi level of the graphene changes accordingly. As a result, the potential barrier gets lower so that the photocarriers injection from the silicon layer to the graphene sheet becomes easier and the transport coefficient η_T increases. This way the carrier concentration in the graphene sheet increases quickly as the pump power increases, which results in a quick increase of the modulation depth, as observed in the inset of Figure 4a.

When the pump power is high enough (*e.g.*, >0.1 mW here), the potential barrier becomes almost negligible and the transport coefficient η_T reaches its maximal value (see Supporting Information). When the pump power P_{pump} increases further, a reverse potential barrier will be formed due to the high doping in graphene. This will suppress the carrier transport and the transport coefficient η_T will decrease accordingly, so that the increase of the modulation depth is slower and slower as shown in Figure 4a. Consequently, a maximal modulation depth (~1.1 dB) is obtained around $P_{pump} =$ 18 mW and the saturation phenomenon is observed.

As the generated photocarrier concentration is directly related to the power density of the pump, we characterize the modulation depth of the OIT effect with the power density (see Supporting Information). The result is similar to that for the modulation depth with the pump power, and it shows that the power density to produce a notable OIT effect is very small (*i.e.*, ~2 W/cm^2), due to the unique mechanism of the present OIT effect. Another way to adjust the power density is to keep the pump power unchanged but adjust the light spot size. In contrast with the above case of increasing the pump power with a constant spot size, the generation rate of photocarriers is nearly unchanged in this case, and thus the carrier concentration of graphene and the modulation depth change only very slightly (see Supporting Information).

Changing the wavelength of the pump light changes the absorption in the silicon greatly without significantly affecting the absorption by graphene. When $\lambda_{pump} = 970$ nm, the modulation depth becomes smaller when compared to the case with the 635 nm pump light due to the weaker absorption coefficient of the 970 nm pump light in silicon (see Supporting Information). Figure 4b shows the modulation depth for the case of $\lambda_{pump} = 970$ nm as the power increases from 0 to 50 mW. It can be seen that the power dependence of the modulation depth for $\lambda_{pump} =$ 970 nm is similar to that for $\lambda_{pump} = 635$ nm (shown in Figure 4a). The pump light of $\lambda_{pump} = 1550$ nm was used as well. According to the chemical potential (−0.24 ~ −0.28 eV) of graphene, the 1550 nm pump light is absorbable for graphene only (because silicon is transparent in this wavelength range), and thus, photocarriers are generated in graphene only. In this case, no OIT effect is observed in our experiment. This again

verifies that the generation of photocarriers in silicon is necessary for producing the present OIT effect.

The temporal responses for the rising and decaying processes of the probe light pulse generated when the pump light (λ_{pump} = 635 nm) illumination is switched on and off were also measured. According to the theoretical calculation of the OIT effect (see Supporting Information), we consider the following two processes to analyze and fit the temporal responses: the carrier transport through the silicon-graphene junction, and the carrier transport in graphene. The fitted time constants (τ_1 and τ_2 for the pulse rising, τ_1' and τ_2' for the pulse decaying) are given in Figure 4c, which shows that there is a slow process and a fast process for the pulse rising as well as the pulse decaying. Since the carrier lifetime in silicon is much longer than the lifetime of carriers in graphene,[37] the slow time constants, τ_1 and τ_1', represent the carrier transport through the silicon−graphene junction, while the fast time constants, τ_2 and τ_2', describe the carrier transport in graphene. This is similar to that observed in a graphene-based PbS quantum-dot infrared photodetector.[32] From Figure 4c, it can be seen that both the slow time constant τ_1 (τ_1') and the fast time constant τ_2 (τ_2') are sensitive to the pump power P_{pump}. We also note that they both have a significant decrease when the pump power increases from 0 to 0.1 mW. According to the above discussion of Figure 4a, this is because the transport coefficient η_T increases significantly when P_{pump} increases from 0 to 0.1 mW, and it reaches the maximal value with almost negligible potential barrier of the silicon−graphene junction when $P_{pump} \approx$ 0.1 mW.

CONCLUSIONS

In summary, we have demonstrated a significant OIT effect in graphene−silicon hybrid photonic integrated circuits for the first time. It has been shown that the OIT effect is caused by the carrier-concentration enhancement in graphene resulting from the photocarrier transport through the silicon−graphene junction. Because the mechanism involves absorption by the silicon, the pump power required to generate the OIT effect is as low as ~0.1 mW and the corresponding power density is about 2 W/cm^2, which is several orders lower than that needed for the saturated absorption of graphene reported before. Furthermore, the OIT effect has been observed not only for local pump-light illumination but also for nonlocal illumination, which enables remote, all-optical control on a chip. By utilizing the present OIT effect, the graphene−silicon hybrid nanophotonic wires could be useful for all-optical, remote, broadband control and sensing, modulation and switching because the present OIT effect is not sensitive to the probe light wavelength. Moreover, the OIT effect also suggests a new and efficient approach to optically tuning the carrier concentration (doping level) in graphene. To achieve an enhanced OIT effect in the hybrid nanophotonic wires for improving the modulation depths as well as the temporal responses, a potential way is patterning the graphene sheet to have a reduced area so that the carrier concentration in the graphene can be increased. Multilayered graphene and chemical/electrical doping of the silicon or graphene might also be helpful to improve the modulation depth of the OIT effect.

METHODS

The fabrication process starts with an SOI wafer, which has a 3 μm-thick buried oxide layer and a 240 nm-thick top silicon layer. The doping type and doping level of the silicon layer is characterized with the SIMS measurement (see Supporting Information). It can be seen that the doping is p-type and the doping level is $\sim 3 \times 10^{14}$ cm^{-3}. The patterns of SOI nanowires are formed by electron-beam lithography (EBL) and inductive coupling plasma (ICP) etching. To achieve efficient coupling of the probe light between the fiber and the chip, each 520 nm-wide SOI nanowire connects with 10 μm-wide grating couplers at its input and output ends through 200 μm-long adiabatic tapers.[38]

To obtain a clean graphene−silicon interface, a BOE (buffered oxide etchant) wet-etching process is used to remove the native SiO_2 layer on the silicon layer. A new ultrathin (~1 Å) SiO_2 layer might be formed quickly afterward because of exposure in air. A large-size (about 1 cm × 1 cm) graphene sheet grown by chemical vapor deposition (CVD) is then wet-transferred onto the SOI chip,[27,29] without requiring any precise alignment. A dry-etching process with oxygen plasma is then applied to remove the graphene covering the regions including the 10 μm-wide grating couplers as well as their 200 μm-long adiabatic tapers. Finally, a 220 nm-thick poly(methyl methacrylate) (PMMA) film is spin-coated onto the wafer to protect the patterned graphene from damage or contamination.

Conflict of Interest: The authors declare no competing financial interest.

Acknowledgment. The authors acknowledge valuable discussions with J. Evans, Z. Wang, L. Liu, D. Liang, W. Guo, and J. E. Bowers. The authors acknowledge funding support from an 863 project (2011AA010301), NSFC projects (61422510, 60990322, 11374263, 61178062, 91233208), Zhejiang provincial grant (2011C11024) of China, the Science and Technology Department of Zhejiang Province (2010R50007), and the Fundamental Research Funds for the Central Universities.

Supporting Information Available: Details of SIMS measurement of the silicon layer, Raman spectroscopy of graphene, measurement and simulation for the propagation loss of the graphene−silicon hybrid nanophotonic wires, responses for different pump power density and different pump wavelength, theoretical calculations of the OIT effect for temporal responses and the graphene−silicon junction. This material is available free of charge *via* the Internet at http://pubs.acs.org.

REFERENCES AND NOTES

1. Novoselov, K. S.; Geim, A. K.; Morozov, S. V.; Jiang, D.; Zhang, Y.; Dubonos, S. V.; Grigorieva, I. V.; Firsov, A. A. Electric Field Effect in Atomically Thin Carbon Films. *Science* **2004**, *306*, 666–669.

2. Geim, A. K.; Novoselov, K. S. The Rise of Graphene. *Nat. Mater.* **2007**, *6*, 183–191.
3. Bonaccorso, F.; Sun, Z.; Hasan, T.; Ferrari, A. C. Graphene Photonics and Optoelectronics. *Nat. Photonics* **2010**, *4*, 611–622.
4. Bao, Q. L.; Loh, K. P. Graphene Photonics, Plasmonics, and Broadband Optoelectronic Devices. *ACS Nano* **2012**, *6*, 3677–3694.
5. Bolotin, K. I.; Sikes, K. J.; Jiang, Z.; Klima, M.; Fudenberg, G.; Hone, J.; Kim, P.; Stormer, H. L. Ultrahigh Electron Mobility in Suspended Graphene. *Solid State Commun.* **2008**, *146*, 351–355.
6. Du, X.; Skachko, I.; Barker, A.; Andrei, E. Y. Approaching Ballistic Transport in Suspended Graphene. *Nat. Nanotechnol.* **2008**, *3*, 491–495.
7. Vakil, A.; Engheta, N. Transformation Optics Using Graphene. *Science* **2011**, *332*, 1291–1294.
8. Hendry, E.; Hale, P. J.; Moger, J.; Savchenko, A. K.; Mikhailov, S. A. Coherent Nonlinear Optical Response of Graphene. *Phys. Rev. Lett.* **2010**, *105*, 097401.
9. Gu, T.; Petrone, N.; McMillan, J. F.; van der Zande, A.; Yu, M.; Lo, G. Q.; Kwong, D. L.; Hone, J.; Wong, C. W. Regenerative Oscillation and Four-Wave Mixing in Graphene Optoelectronics. *Nat. Photonics* **2012**, *6*, 554–559.
10. Liao, L.; Lin, Y. C.; Bao, M. Q.; Cheng, R.; Bai, J. W.; Liu, Y. A.; Qu, Y. Q.; Wang, K. L.; Huang, Y.; Duan, X. F. High-Speed Graphene Transistors with a Self-Aligned Nanowire Gate. *Nature* **2010**, *467*, 305–308.
11. Wang, F.; Zhang, Y. B.; Tian, C. S.; Girit, C.; Zettl, A.; Crommie, M.; Shen, Y. R. Gate-Variable Optical Transitions in Graphene. *Science* **2008**, *320*, 206–209.
12. Xia, F. N.; Mueller, T.; Lin, Y. M.; Valdes-Garcia, A.; Avouris, P. Ultrafast Graphene Photodetector. *Nat. Nanotechnol.* **2009**, *4*, 839–843.
13. Mueller, T.; Xia, F. N.; Avouris, P. Graphene Photodetectors for High-Speed Optical Communications. *Nat. Photonics* **2010**, *4*, 297–301.
14. Li, X. M.; Zhu, H. W.; Wang, K. L.; Cao, A. Y.; Wei, J. Q.; Li, C. Y.; Jia, Y.; Li, Z.; Li, X.; Wu, D. H. Graphene-on-Silicon Schottky Junction Solar Cells. *Adv. Mater.* **2010**, *22*, 2743–2748.
15. Chen, C. C.; Aykol, M.; Chang, C. C.; Levi, A. F. J.; Cronin, S. B. graphene−silicon Schottky Diodes. *Nano Lett.* **2011**, *11*, 1863–1867.
16. Liu, M.; Yin, X. B.; Ulin-Avila, E.; Geng, B. S.; Zentgraf, T.; Ju, L.; Wang, F.; Zhang, X. A Graphene-Based Broadband Optical Modulator. *Nature* **2011**, *474*, 64–67.
17. Liu, M.; Yin, X. B.; Zhang, X. Double-Layer Graphene Optical Modulator. *Nano Lett.* **2012**, *12*, 1482–1485.
18. Bao, Q. L.; Zhang, H.; Ni, Z. H.; Wang, Y.; Polavarapu, L.; Shen, Z. X.; Xu, Q. H.; Tang, D. Y.; Loh, K. P. Monolayer Graphene as a Saturable Absorber in a Mode-Locked Laser. *Nano Res.* **2011**, *4*, 297–307.
19. Bao, Q. L.; Zhang, H.; Wang, Y.; Ni, Z. H.; Yan, Y. L.; Shen, Z. X.; Loh, K. P.; Tang, D. Y. Atomic-Layer Graphene as a Saturable Absorber for Ultrafast Pulsed Lasers. *Adv. Funct. Mater.* **2009**, *19*, 3077–3083.
20. Hochberg, M.; Baehr-Jones, T. Towards Fabless Silicon Photonics. *Nat. Photonics* **2010**, *4*, 492–494.
21. Asghari, M.; Krishnamoorthy, A. V. Silicon Photonics: Energy-Efficient Communication. *Nat. Photonics* **2011**, *5*, 268–270.
22. Gan, X. T.; Shiue, R. J.; Gao, Y. D.; Meric, I.; Heinz, T. F.; Shepard, K.; Hone, J.; Assefa, S.; Englund, D. Chip-Integrated Ultrafast Graphene Photodetector with High Responsivity. *Nat. Photonics* **2013**, *7*, 883–887.
23. Pospischil, A.; Humer, M.; Furchi, M. M.; Bachmann, D.; Guider, R.; Fromherz, T.; Mueller, T. CMOS-Compatible Graphene Photodetector Covering All Optical Communication Bands. *Nat. Photonics* **2013**, *7*, 892–896.
24. Wang, X. M.; Cheng, Z. Z.; Xu, K.; Tsang, H. K.; Xu, J. B. High-Responsivity Graphene/Silicon-Heterostructure Waveguide Photodetectors. *Nat. Photonics* **2013**, *7*, 888–891.
25. Cheng, Z. Z.; Tsang, H. K.; Xu, K.; Shi, Z. R. Spectral Hole Burning in Silicon Waveguides with a Graphene Layer on Top. *Opt. Lett.* **2013**, *38*, 1930–1932.
26. Li, H.; Anugrah, Y.; Koester, S. J.; Li, M. Optical Absorption in Graphene Integrated on Silicon Waveguides. *Appl. Phys. Lett.* **2012**, *101*, 111110.
27. Suk, J. W.; Kitt, A.; Magnuson, C. W.; Hao, Y. F.; Ahmed, S.; An, J. H.; Swan, A. K.; Goldberg, B. B.; Ruoff, R. S. Transfer of CVD-Grown Monolayer Graphene onto Arbitrary Substrates. *ACS Nano* **2011**, *5*, 6916–6924.
28. Schroder, D. K.; Thomas, R. N.; Swartz, J. C. Free Carrier Absorption in Silicon. *IEEE J. Solid-State Circuits* **1978**, *13*, 180–187.
29. Yu, L. H.; Xu, Y.; Shi, Y. C.; Dai, D. X. Linear and Nonlinear Optical Absorption of On-Chip Silicon-on-Insulator Nanowires with Graphene. Presented at Asia Communications and Photonics Conference, Guangzhou, China, November 7−10, **2012**; AS1B.3.
30. An, Y. B.; Behnam, A.; Pop, E.; Ural, A. Metal-Semiconductor-Metal Photodetectors Based on Graphene/p-Type Silicon Schottky Junctions. *Appl. Phys. Lett.* **2013**, *102*, 013110.
31. Sze, S. M.; Ng, K. K. *Physics of Semiconductor Devices*, 3rd ed.; John Wiley & Sons: Hoboken, NJ, 2007.
32. Sun, Z. H.; Liu, Z. K.; Li, J. H.; Tai, G. A.; Lau, S. P.; Yan, F. Infrared Photodetectors Based on CVD-Grown Graphene and PbS Quantum Dots with Ultrahigh Responsivity. *Adv. Mater.* **2012**, *24*, 5878–5883.
33. Das, A.; Pisana, S.; Chakraborty, B.; Piscanec, S.; Saha, S. K.; Waghmare, U. V.; Novoselov, K. S.; Krishnamurthy, H. R.; Geim, A. K.; Ferrari, A. C.; *et al.* Monitoring Dopants by Raman Scattering in an Electrochemically Top-Gated Graphene Transistor. *Nat. Nanotechnol.* **2008**, *3*, 210–215.
34. Jnawali, G.; Rao, Y.; Yan, H. G.; Heinz, T. F. Observation of a Transient Decrease in Terahertz Conductivity of Single-Layer Graphene Induced by Ultrafast Optical Excitation. *Nano Lett.* **2013**, *13*, 524–530.
35. Li, X. S.; Cai, W. W.; An, J. H.; Kim, S.; Nah, J.; Yang, D. X.; Piner, R.; Velamakanni, A.; Jung, I.; Tutuc, E.; *et al.* Large-Area Synthesis of High-Quality and Uniform Graphene Films on Copper Foils. *Science* **2009**, *324*, 1312–1314.
36. Kim, Y. D.; Bae, M.-H.; Seo, J.-T.; Kim, Y. S.; Kim, H.; Lee, J. H.; Ahn, J. R.; Lee, S.; Chun, S.-H.; Park, Y. D. Focused-Laser-Enabled p-n Junctions in Graphene Field-Effect Transistors. *ACS Nano* **2013**, *7*, 5850–5857.
37. Cheng, Z.; Tsang, H. K.; Wang, X.; Xu, K.; Xu, J.-B. In-Plane Optical Absorption and Free Carrier Absorption in Graphene-on-Silicon Waveguides. *IEEE J. Sel. Top. Quantum Electron.* **2014**, *20*, 4400106.
38. Taillaert, D.; Laere, F. V.; Ayre, M.; Bogaerts, W.; Thourhout, D. V.; Bienstman, P.; Baets, R. Grating Couplers for Coupling between Optical Fibers and Nanophotonic Waveguides. *Jpn. J. Appl. Phys.* **2006**, *45*, 6071–6077.